Overscreening, Coion-Dominated Electroosmosis, and Electric Field Strength Mediated Flow Reversal in Polyelectrolyte Brush Functionalized Nanochannels

Turash Haque Pial, Harnoor Singh Sachar, Parth Rakesh Desai, and Siddhartha Das*

Department of Mechanical Engineering, University of Maryland, College Park, MD-20742, USA

*Email: sidd@umd.edu

Abstract:

Controlling the direction and strength of nanofluidic electrohydrodyanmic transport in presence of an externally applied electric field is extremely important in a number of nanotechnological applications. Here, we employ all-atom molecular dynamics (MD) simulations to discover the possibility of changing the direction of electroosmotic (EOS) liquid flows by merely changing the electric field strength in a nanochannel functionalized with polyelectrolyte (PE) brushes. In exploring this, we have uncovered three facets of nanoconfined PE brush behavior and resulting electroosmotic (EOS) transport. First, we identify the onset of an overscreening effect: such overscreening refers to the presence of more counterions (Na^+) within the brush layer than needed to neutralize the negative brush charges. Accordingly, as a consequence of the overscreening, in the bulk liquid outside the brush layer, there is a greater number of coions (Cl^-) than counterions in the presence of an added salt (NaCl). Second, this specific ion distribution ensures that the overall EOS flow is along the direction of motion of the coions. Such coion-dictated EOS transport directly contradicts the notion that EOS flow is always dictated by the motion of the counterions. Finally, for large-enough electric fields, the brush height reduces significantly enforcing some of the excess overscreening-inducing counterions to squeeze out of the PE brush layer into the brush-free bulk. As a result, the overscreening effect disappears and the number of coions and counterions outside the PE brush layer becomes similar. Despite that there is an EOS transport: this EOS transport, unlike the standard EOS transport that occurs due to the imbalance of the coions and counterions, occurs since a larger residence time of the water molecules in the first solvation shell of the counterions (Na^+) ensures a water transport in the direction of motion of the counterions. The net effect is the reversal of the direction of the EOS transport by merely changing the strength of the electric field.

Keywords: electroosmotic flow, overscreening, polyelectrolyte brush, flow reversal, molecular dynamics simulation, nanochannel.

In nanofluidic transport of liquids, ions, and (bio)particles, application of electrokinetics span a large range of disciplines from geoscience,[1] energy engineering,[2,3] sensing and separation,[4,5] gating of ions and liquids[6,7] to advancing biomimetic and bioinspired engineering.[8,9] Electroosmotic (EOS) flow, a type of electrokinetic transport, can be generated in a micro-nanochannel by applying an external electric field to drive the ion-containing (electrolyte) liquids. In some practical scenarios, the direction of EOS flow inside the nanochannel (positive or negative, relative to the applied electric field) needs to be manipulated in a way that enhances mixing, reaction, separation, and printing.[10-14] Previous research has shown that one needs to modify the system's overall environment to get a modified flow behavior. For example, changing the sign of the zeta potential or the surface charge density of the channel wall,[15,16] or controlling the buffer pH value[17] may help to control the EOS flow direction in some simplified systems. Reversed and patterned flows inside a nanochannel can also be induced by suitable surface modifications.[18,19] These experimental studies have been supplemented by atomistic simulation studies on modulating nanochannel EOS flows by changing the surface charge density or hydrophobicity of the channel wall.[20,21] All of these modifications eventually change the mobile ion distribution in the nanochannel, which in turn leads to different flow directions inside the nanochannel. Therefore, in order to control the direction of the EOS transport in a nanochannel by merely changing the strength of the driving electric field, one needs to trigger a situation where the ion distribution (or more generally, the mechanism that drives the EOS transport) gets altered by the variation in the strength of the electric field. To the best of our knowledge, such a scenario has rarely been accomplished.

Surfaces grafted with polyelectrolyte (PE) brushes[22] are well-known for their responsiveness to different environmental stimuli and have been used in a myriad of applications like ion and bioanalayte sensing,[23,24] fabrication of ionic diodes,[25,26] nanofluidic current rectification,[27,28] oil recovery,[29] targeted nanoparticle-based delivery[30,31] *etc*. Such grafting with PE brushes has also enabled functionalizing nanochannels for applications in sensing and current rectification. The applied axial electric field will invariably cause an EOS transport in such brush-grafted, electrolyte-solution filled nanochannels given the fact that the charged brushes develop their own mobile ion distribution around them neutralizing their charges and this ion distribution respond to the applied electric field. In fact, the response of the PE brushes to the applied electric field and the resulting changes in the morphology of the brushes and the associated ion distribution makes it possible to significantly influence the EOS transport in brush-grafted nanochannels. Despite its tremendous potential, EOS flow in PE-brush-grafted nanochannels has not been well studied in an atomistically-resolved scale. Along with a few simplified continuum studies,[32,33] there are only a handful of MD simulation studies available for liquid transport in brush-grafted nanochannels.[34-37] However, none of these studies have considered an all-atom description of the brushes and solvent molecules, which can be important in obtaining the appropriate brush, water and ion behavior in PE brush grafted system, and therefore providing an atomisticially-resolved description of such EOS transport in brush-functionalized nanochannels.[38]

In this paper, we have studied the EOS transport in nanochannels functionalized with PE brushes in an all-atom MD setup that couples the PE brush system with an external electric field. We first discover that for zero to intermediate electric field strengths the large confinement enforces an overscreening effect, which implies the presence of more number of counterions within the PE brush layer than that required to screen the PE charges. Second, as a result of such

overscreening, the number of coions (from the added salt) is larger than the number of counterions within the brush-free bulk. As a result, in conjunction with the fact that the flow within the brushes is severely retarded, the EOS flow for small and medium strength electric fields is in the same direction as the motion of the coions. Such coion-dictated EOS transport is a most intriguing of finding, given the fact that the EOS transport is always believed to occur in the direction of the counterions. Finally, for larger electric fields, the brush height is significantly reduced enforcing a reduction in the overscreening effect and creating parity in the number of coions and counterions within the brush-free bulk. Therefore, the EOS transport does not occur to the imbalance of the counterions and coions. On the contrary, we establish that the residence time of the water molecules is larger within the first hydration shell of the considered counterions (Na^+) than the coions (Cl^-): we hypothesize that the EOS transport is triggered by this difference of the residence time and accordingly, occurs in the direction of the motion of the counterions. These circumstances enable us to obtain the situation where there is an electric field strength mediated reversal in the direction of the EOS transport in nanochannels functionalized with PE brushes.

Results and Discussions

Overscreening, coion-directed electroosmotic flow, and electric field strength mediated flow reversal

In our system [shown in Fig. 1(A)], fully ionized Polyacrylic acid (PAA) chains (H[-CH_2-$CH(COO^-)$-]nCH3) are used as the polyelectrolytes and explicitly modeled water molecules act as the solvent. Sodium counterions (Na^+ ions) are added to neutralize the PE segmental charge. In addition, 0.1 M NaCl salt is added to the system. All other details associated with the simulation are provided in method section in this article and section S1 of the Supporting Information (SI).

For driving the flow in the PAA-brush-grafted nanochannel, we applied electric field whose strengths ranged from 0.1 to 1 V/nm in axial (or x) direction. While such large electric fields are not routinely employed in experiments,[39-41] it is possible to generate electric fields in the range of 1-5 V/nm for certain applications.[42] In fact, several experimentally probed biological problems involving proteins and DNA have considered electric fields in the order of 0.1-1 V/nm. For example, there have been studies probing the behavior of protein cytochrome c immobilized on silver electrodes in the presence of electric fields that were calculated to be in the range of 1-2.5 V/nm.[43] Similarly, Heng *et al*. probed the electromechanics of a DNA molecule in a synthetic nanopore in the presence of an electric field of 0.31 V/nm.[44] Furthermore, such large electric fields are needed for the typical MD simulation studies[34-36] for suppressing the thermal noise in order to increase the signal-to-noise ratio. It is also interesting to note here that the threshold value of the electric field strength that triggers the initiation of the water ionization has been reported to be around 2.5 V/nm and the ionization becomes more frequent around an applied electric field of 3.5 V/nm,[45,46] which is several times higher than the electric field strength (0.1-1 V/nm) considered in our simulations. When an electric field $\boldsymbol{E}$ is applied to the system, a force of $q_i\boldsymbol{E}$ acts on the atom

i having a charge of q_i. In figure 1(B), we depict the electroosmotic (EOS) velocity profiles (*i.e.*, the velocity profiles of the water molecules) as a function of the applied electric field. The following key results emerge: (1) for smaller magnitude of electric fields ($|\boldsymbol{E}|$=0.1, 0.5 V/nm), the EOS flow occurs in the direction opposite to the applied electric field (negative *x* direction or the direction in which the coions move, see later), (2) for larger electric field ($|\boldsymbol{E}|$=1 V/nm), the direction of the EOS flow is reversed, *i.e.*, water flows in the same direction as the applied electric field (positive *x* direction or the direction in which the counterions move, see later), and (3) for all the electric fields, the EOS flow occurs primarily outside the brushes, while the flow inside the brushes is very small. These EOS velocity profiles, therefore, confirm a coion-dictated EOS flow for small electric fields (the standard EOS flow is invariably counterion-dictated) and an electric field strength driven reversal in the direction of the EOS flow profile (usually the EOS flow increases in strength, but never reverses, with an increase in electric field strength). In the rest of this article, we shall try to identify the fundamental factors responsible for such highly non-intuitive EOS transport in brush-functionalized nanochannels.

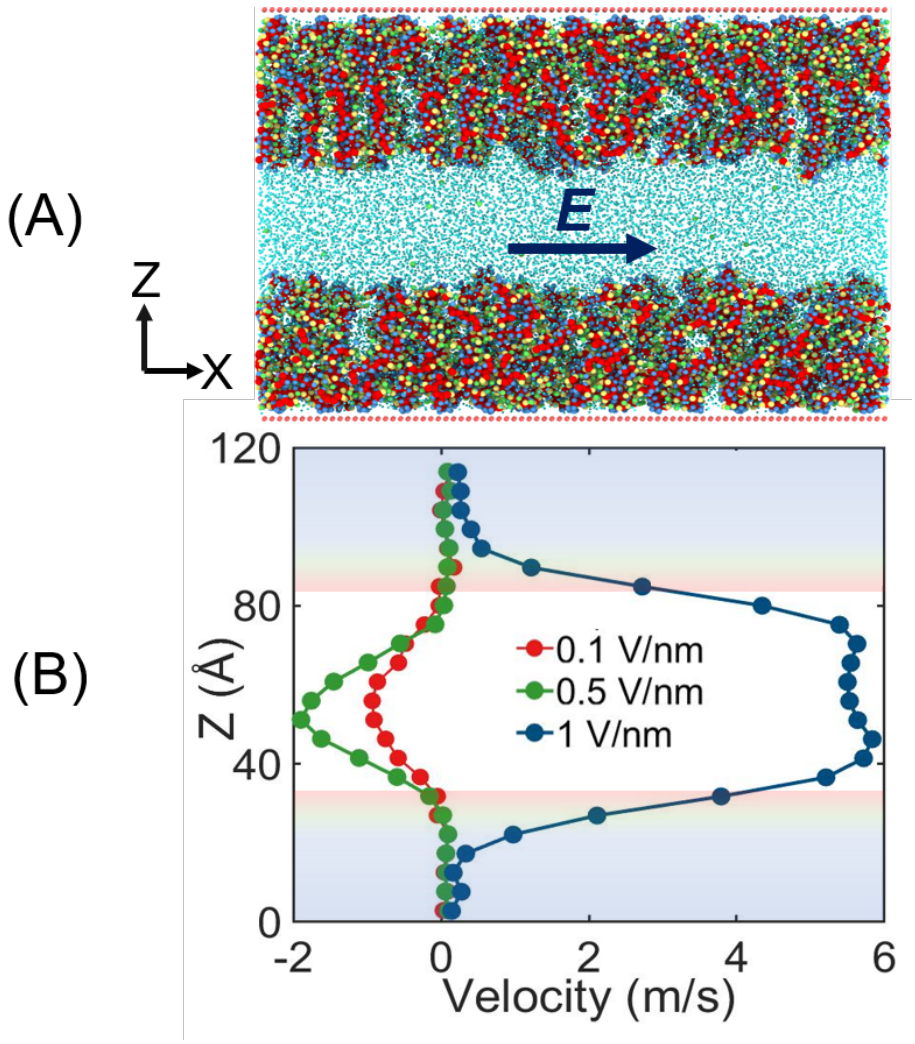

Figure 1: (A) A schematic of the PE brush grafted nanochannel system. (B) Velocity of the water (solvent) molecules along the system height for different electric fields.

We first study the distribution of the coions (resulting from the added salt) and counterions (resulting from the added salt and charge neutralizing counterions) inside and outside the brush layer for different electric field strengths. We clearly find that for no or small electric fields, there is an overscreening effect within the brushes, quantified by the presence of a larger number of counterions than needed to screen the PE charges [see Fig. 2(A) and Table S8 in the SM]. This excess counterions come from the added salt: accordingly, the number of coions will be greater than the number of counterions in the brush-free bulk [see Fig. 2(A) and Table S8]. This is also evident from the spatial distribution of the coions and counterions for $|\boldsymbol{E}|$ = 0.1 V/nm [see Fig. 2(B)]. The significantly larger concentration of the Cl^- ions (coions) in the bulk ensures that net direction of the motion of the solvent will be in the direction of the motion of the coions, leading to the case of coion-dominated EOS transport for lower applied electric field. For a larger electric field, *i.e.*, $|\boldsymbol{E}|$ =1 V/nm on the other hand, we find a significant reduction in the overscreening effect within the PE brush layer, leading to an almost equal number of coions and counterions within the brush-free bulk [see Figs. 2(A,C) and Table S8].

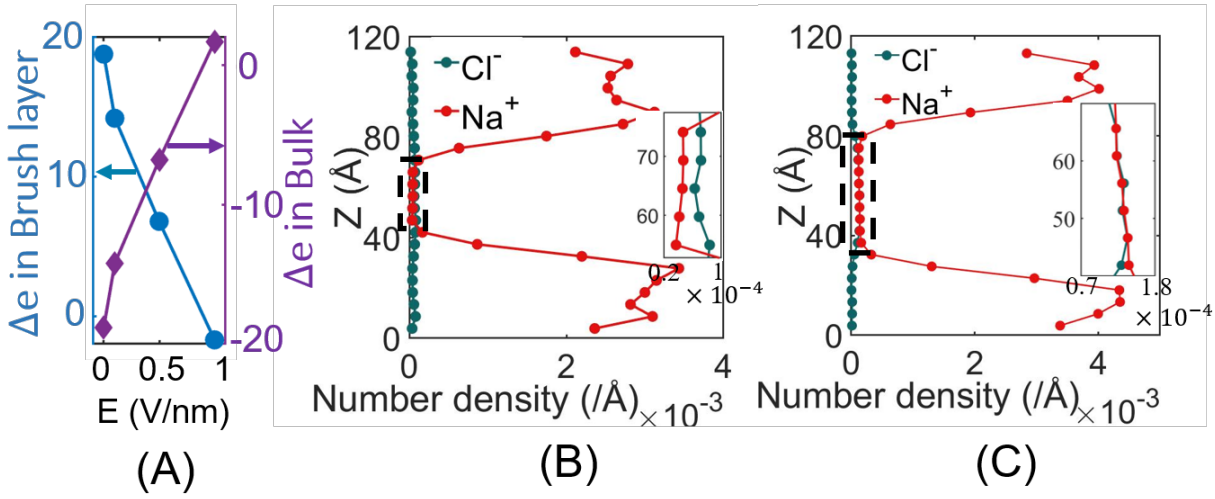

Figure 2: (A) Excess of the positive charges $\Delta e = (e_+ - e_-)$ inside brush and in brush-free bulk as a function of the electric field. e_+ and e_- indicate total number of positive charges (Na^+) and negative charges (Cl^- and PE charges) respectively. Number density of ions in the system for electric field strength of (B) 0.1 V/nm, and (C) 1 V/nm. In the insets of (B) and (C), the number density of ions (having the same unit as the main figure) near the bulk region have been zoomed. Please see Fig. S6(A) for the ion number distribution for $|\boldsymbol{E}|$=0.5 V/nm.

In order to understand such non-intuitive electric field mediated disappearance of the overscreening effect, which will also affect the direction of the EOS transport, we study the response of the PE brushes to the electric field. We find that there is an overall reduction in the vertical end-to-end brush height with an increase in the electric field strength [see Fig. 3(A)]. Previously, Netz showed the unfolding of a PE globule to a rod-like chain under applied electric fields:[47,48] this knowledge will help us to explain brush height reduction with electric field. In these studies,[47,48] without an electric field, the PE is neutralized by counterions to form a PE-counterion globule. Applied electric filed tends to orient the counterion distribution around the PE and a net dipole-moment is induced in the PE-counterion complex in the direction of the electric field. This finite dipole moment (which also indicates a polarization) tends to orient a coil or unfold a globule to a rod-like chain that aligns in the direction of the electric field.[47,48] In this study, COO^- are the functional groups of the PAA PE molecule, which are neutralized by the counterions. We first obtain the probability of finding a counterion around the oxygen atoms of the COO^- groups [see Fig. 3(B) and Fig. S4]. For the case of $|\boldsymbol{E}|$=1 V/nm, the counterions prefer to localize on the positive side ($X > 0$; note that $\boldsymbol{E}$ is directed from $X < 0$ to $X > 0$) of these oxygen atoms. However, no such direction-dependent preference is observed for the case where no electric field is applied. This electric field mediated orientation of O^--Na^+ ion-pair indicates that we enforce a directional dependence of the charge distribution, which is similar to the induced dipole moment identified previously.[47-49] Therefore, we can infer that this aligned ion-pair will try to align the brush in the applied electric field direction. To verify this, we study the probability distribution of monomer in *x* and *y* directions: for that purpose, we consider the position of grafted carbon atom as center (0,0) and count the number of backbone carbon atoms in *x* and *y* directions around (0,0). We can see that in the *x* direction, monomers become sparser which means they become aligned in *x* direction

[see Fig. 3(C,top)], while no such change is observed in the probability of finding monomer in the *y* direction [see Fig. 3(C,bottom)]. Therefore, we can infer that due to the electric field driven alignment of the ion pairs in *x* direction, polymers tend to be aligned in the *x* direction, which eventually reduces the brush height in *z* direction and increases the effective volume of the brush-free region [shown schematically in Fig. 3(D)]. As a consequence, there is a lesser available volume for the ions within the brush layer, enforcing a squeezing-out (or exclusion) of primarily most of the overscreening causing counterions (and a few coions, especially for very large $|\boldsymbol{E}|$, see Table S8 in the SI) from within the brush-layer to the bulk: this explains the reduction in overscreening (or attaining a parity in the number of coions and counterions within the brush-free bulk) with an increase in the strength of $|\boldsymbol{E}|$.

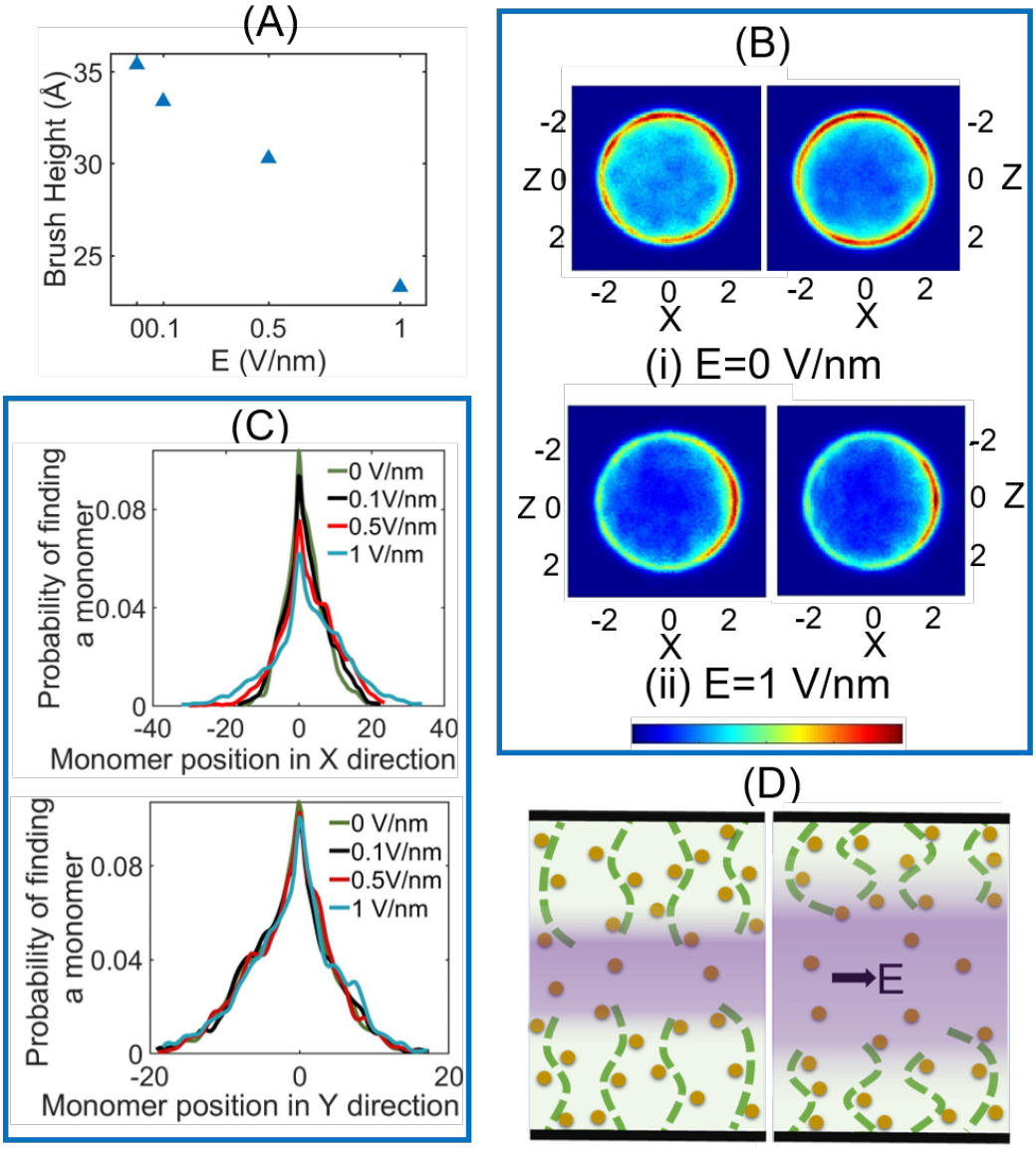

Figure 3: (A) End to end brush height as a function of applied electric field (also see Fig. S3 in the SI). (B) Na^+ ion distribution contour around an O^- of COO^- for $|\boldsymbol{E}| = 0$ and $|\boldsymbol{E}| = 1$ V/nm. Colorbar indicates concentration from low to high (blue to red). (C) Probability distribution of finding a backbone carbon in x and y direction under different electric field strength. (D) An illustration showing the electric field induced reduction in brush height also causing an increase in the volume of the brush-free region (shown in purple). In (D), dashed lines and circles represent PE chains and counterions, respectively.

In addition to the difference in the ion concentration distributions, the electric field dependent velocities of the Na^+ and Cl^- ions are also important for quantifying the electric field dependent EOS flow profiles. Fig. 4(A) and Fig. S6(B) (see the SI) establish that the velocity of the Cl^- ions is larger than the velocity of Na^+ ions at low electric field strengths ($|\boldsymbol{E}|$=0.1, 0.5 V/nm), while at larger electric field ($|\boldsymbol{E}|$=1 V/nm) the velocity of the two ions are similar [see Fig. 4(B)]. Previous studies have shown that at low electric field strength, the mobility of Cl^- ions is higher than the mobility of the Na^+ ions[50] and this difference in the mobility reduces on increasing the electric field strength. This justifies the significantly larger velocities of the Cl^- ion for $|\boldsymbol{E}|$=0.1, 0.5 V/nm and similar velocities of the Cl^- and Na^+ ions for $|\boldsymbol{E}|$=1 V/nm. Results from experiments[51] are also consistent with our MD simulation predictions for smaller $|\boldsymbol{E}|$ values. This higher velocity coupled with a larger concentration of Cl^- for smaller $|\boldsymbol{E}|$ also drives the EOS flow along the direction of the coion at low electric field strengths.

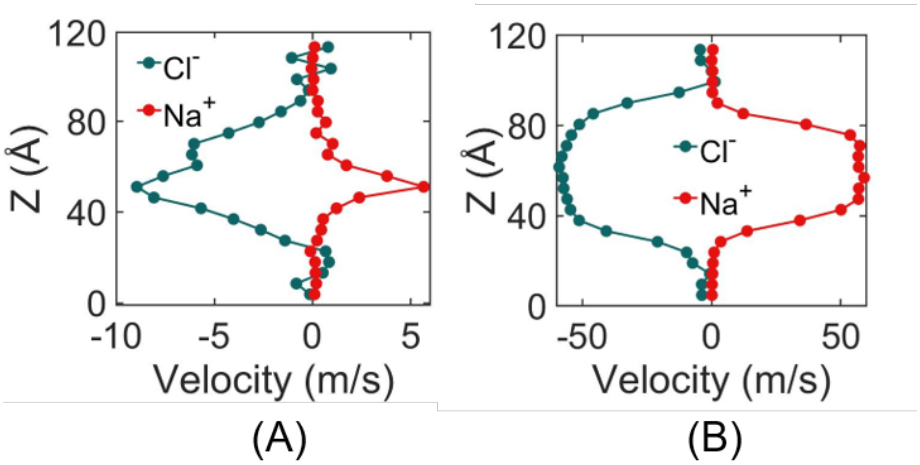

Figure 4: Velocity profiles of ions for (A) $|\boldsymbol{E}|$ = 0.1 V/nm and (B) $|\boldsymbol{E}|$ = 1 V/nm.

We finally quantify the strength of the dynamic interaction of the water molecules with the ions: such quantification is essential to pinpoint the extent to which the overall flux of the ions (which is a combination of its concentration and the mobility/velocity) dictates the EOS velocity of the water. This dynamic interaction is quantified by calculating the average residence time of a water molecule (oxygen atom) within the first solvation shell of ion [which closely resembles interaction strength (hydration free energy)].[52] The residence times [R(t)] are calculated from the time correlation function defined as:

$$R(t) = \frac{1}{N_h}\sum_{i=1}^{N_h} \theta_i(t_0)\theta_i(t_0 + t). \qquad (1)$$

Here θ_i is the Heaviside unit step function (if one water molecule i resides inside the first solvation shell of an ion, θ_i =1; otherwise, θ_i =0), N_h is the number of water molecules in the first solvation shell (the radial distribution functions needed for calculating solvation shell size have been provided in the SI, please see Fig. S7), and t_0 is the initial time step. This residence time is averaged for all ions in the bulk and over 50 different initial time steps. Fig. 5 shows that for both small and large electric fields, the residence time of water in the first hydration shell of the Na^+ ion is much larger than that of the Cl^- ion, which implies that the water molecules reside for much longer within the Na^+ solvation shell allowing the Na^+ ions to drag the water molecules with them for much longer. On the other hand, for Cl^- ion, where this timescale is smaller, water can diffuse out of the solvation shell of the Cl^- ion much faster, and can be dragged for lesser time. Therefore, for large field strengths where both the bulk concentration as well as the velocities are very similar for the Na^+ and Cl^- ions, this significantly larger residence time for the Na^+ ion ensures that the water molecules will preferentially move in the direction in which the Na^+ ion moves: accordingly, we find that the EOS flow is counterion-dictated. On the other hand, for smaller electric field strengths,

the larger bulk concentration and velocity of the Cl^- ions overwhelm the effect of smaller residence time leading to the water transport and the EOS flow to be coion-dictated. Finally, the very small EOS velocity inside the brushes [as compared to the bulk region, see Fig. 1(B)] can be explained by noting that the motion of the counterions inside the brush layer is severely hindered due to the fact that the positive counterions are bound to the negatively charged PE chains by strong electrostatic forces and the fact that the densely grafted brushes exert a large confinement effect on the brush-supported counterions and water molecules.[38] To explain further, such a large electrostatic attraction between the counterions and the PAA brush molecules ensures that a very large portion of the counterions is condensed on the charged PAA chains, and accordingly, the motion of these condensed counterions is restricted by the motion of the densely grafted PAA chains. Such condensation of ions on charged polymer chains is also known to dictate the mobility of ions in polyelectrolyte gels.[53] Also, as elucidated in our previous study, for densely grafted PAA brushes a large confinement effect is triggered due to a strong steric hindrance effect: as a result, there is a large reduction in the freedom of movement of the ions and water reducing their mobilities within the brush layer.[38]

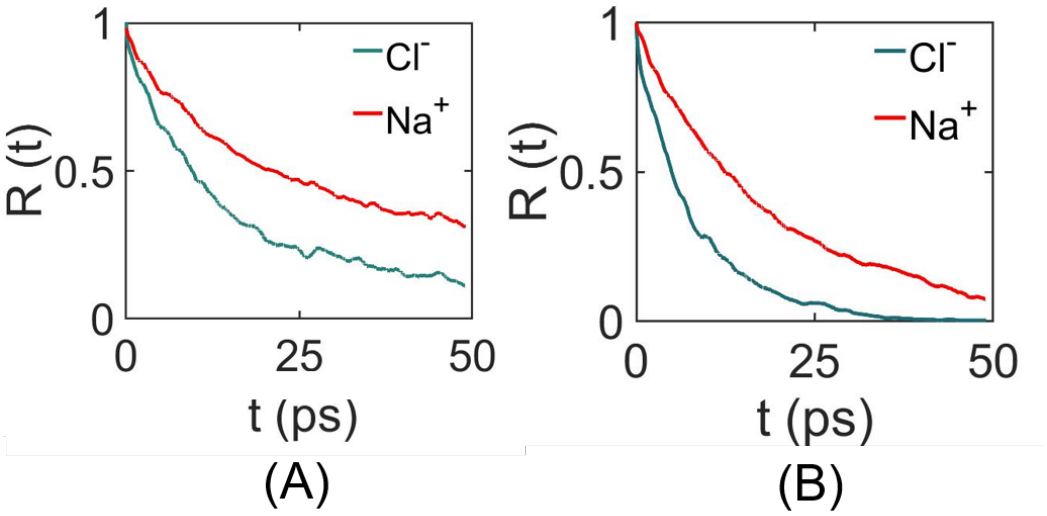

FIG. 5: Residence time correlation function for both ions for (A) $|\boldsymbol{E}|$ = 0.1 V/nm and (B) $|\boldsymbol{E}|$ = 1 V/nm.

Generality and reasoning of overscreening

From the previous subsection, it is clear that the overscreening is the main phenomenon that drives the coion-dominated flow and subsequent electric field strength mediated flow reversal. Before probing the detailed mechanism dictating the occurrence of overscreening, it is useful to probe the generality of the overscreening phenomenon. To check this generality, we have performed a few more simulations with PE brush grafting density, salt concentration, and PE brushes that are different as compared to those studied and discussed in the previous section. The main flow simulations discussed so far is performed in a nanochannel grafted with PAA polyelectrolyte (PE) brushes with a grafting density of $0.05/\sigma^2$ (with Na^+ screening counterions) in presence of 0.1 M NaCl added salt. We have considered three more systems by varying the grafting density (grafting density of $0.03/\sigma^2$), concentration of the added salt (0.2 M of added NaCl salt), and the nature of the PE brushes [nanochannels grafted with Poly-methacrylic acid (PMMA) brushes)]. The details of these simulations can be found in section S5 in the SI. For all these three cases, we have observed overscreening (as confirmed by the ion number density distributions provided in Fig. S9 and values reported in Table S8 in SI). The confirmation of overscreening for these three cases as well as the overscreening for the case reported in the previous subsection establish that the overscreening in a PE brush grafted nanochannel is indeed a generic phenomenon that occurs (with the added NaCl salt) for different PE brush grafting densities, salt concentration, and PE brush type.

To understand the mechanisms responsible for overscreening, we have performed simulations for two more systems. In the first one, PAA brushes are grafted to a single interface (*i.e.*, not a nanochannel) with significantly large bulk volume [see figure 6 (A)]. This is identical to the system considered in our previous study.[38] In the second simulation, the nanochannel is

grafted with PAA brush layers with Cs^+ ions acting as screening counterions and 0.1 M CsF as the added salt. Details of these two simulations can be found in section S6 in the SI. For the ease of explaining in this section, we are referring the main simulation of the previous section with nanoconfinement and NaCl salt as system N1, the system without nanoconfinement as system N2, and the system with nanoconfinement, Cs^+ as screening counterions, and CsF as the added salt as system N3.

Figures 6(B) and 6(D) illustrate the ion distribution profiles for systems N2 and N3. No overscreening is observed in these two cases, which indicates that the presence of nanoconfinement and the types of coions and counterions play critical roles in determining overscreening. Identification of these roles is critical to pinpoint the onset of overscreening.

We identify that overscreening results from interplay of three phenomena. First is the possible lowering of the osmotic pressure caused by the migration of the salt ions from within the bulk to inside nearby brush layer. The second is the dependence of such migration on the sizes of the salt cations and anions. The third is the stabilization (or the lack of it) of the cations within the PE brush layer induced by their strong (or weak) attraction to the COO^- group of the PE brushes. We discuss the occurrences of these three phenomena to different extents in the three systems that we have studied and from that pinpoint the mechanism of overscreening within the PE brush layer for the system N1.

The osmotic pressure (Π) can be simplistically expressed as $\Pi = Nk_BT/V$, where N is the number of non-interacting species and V is the volume where the species are present. For the case of nanochannel grafted with the PE brushes, the bulk volume (*i.e.*, the volume where the brushes are absent) is significantly small. Accordingly, if all the added salt ions (or N) remain confined in this small bulk volume (V), the osmotic pressure will become very large. Therefore, in order to

reduce this large osmotic pressure inside the bulk (with a small volume), some of the salt ions tend to migrate and localize inside the brushes, which is also helped by the fact that all the salt in the nanochannel bulk is in close proximity to the brush layer (on account of the nanochannel induced confinement). This will be true for both the systems N1 and N3. On the other hand, for system N2, where there is no nanochannel and the bulk is significantly more extended, the osmotic pressure in the bulk is not large enough to enforce a migration of the salt ions towards and inside the PE brushes which is not in close proximity to most of the ions. Therefore, in system N2, overscreening is not observed in the absence of nanoconfinement.

As discussed above, for both systems N1 and N3, osmotic pressure in the bulk will drive some salt ions from the bulk to inside the brush layer. The size of the Na^+ ion is smaller than the Cl^- and the size of the Cs^+ is distinctly larger than the F^- ion. Accordingly, there will be a much larger tendency of the Na^+ ions than Cl^-, and F^- ions than Cs^+ to migrate from the bulk to within the PE brush layer. For example, the solvation radii of the different ions considered here are as follow: 3.76 Å for Na^+, 3.84 Å for Cl^-, 4.52 Å for Cs^+, 3.33 Å for F^-. This size-based larger tendency of the Na^+ and F^- ions to enter the PE brush layer is effectively a size-based exclusion (or steric effect). The third and final issue, which also depends on the relative sizes (and hence the charge densities) of the Na^+ and Cs^+ ions (although this is not a size-based exclusion effect), is related to what extent the Na^+ and Cs^+ ions neutralize the O^- of the COO^- group, *i.e.*, form the $–COO^-Na^+$ or $–COO^-Cs^+$ ion pair. Formation of such ion pair, induced by the attraction between opposite charges, is of course energetically very favorable. Larger the extent of this neutralization, larger will be the favorability of the cations (that have entered the PE brush layer) to remain (in a stabilized configuration) within the brush layer. In this regard, we first computed the percentage of $–COO^-$ groups neutralized by the Na^+ ion for system N2 (*i.e.*, without nanoconfinement). In

order to do so, we considered the O of COO^- and checked if one or more Na^+ ions were present inside the first solvation shell of this O or not. We found that around 80% of the O atoms of COO- are neutralized with the help of Na^+ ions, while the remaining O^- atoms were fully surrounded by the hydrogen of water (H_{water}). On the other hand, in the PE-brush-grafted nanochannel case with NaCl as the added salt (*i.e.* system N1), 95.3% of the O atoms of the COO- were neutralized by Na^+ ions. From these two observations, we can infer that in an equilibrium, while it suffices if 80% of the O atoms of COO^- are neutralized by the Na^+ ion, availability of higher number of Na^+ ions within the PE layer makes it feasible for some of these Na^+ to replace the H of water and themselves neutralize the O atoms of the COO^-. The larger charge density of the Na^+ ions ensures that such replacement (and the subsequent formation of the COO^-Na^+ ion pair) is energetically more favorable. All these factors eventually ensure that the PAA brush layer grafted on the inner walls of the nanochannels can have more cations (in a stable configuration) than it requires for being in an equilibrated state, and eventually causes the overscreening. To observe this energy favorability of Na^+ ions within the PE brush layer, we have performed two free energy calculations for system N1. From the free energy curves, we can see that it is distinctly more favorable for the Na^+ ion to remain inside the brush layer [see Fig. 6(C)]. It is also clear that, energy favorability of the Na^+ ion is more around a COO^- functional group (present at Z=-5 Å and Z=-16Å), as confirmed by the presence of the local minima in the plot for these Z values. On the other hand, for Cl^- ion no such energy favorability is observed inside the brush layer. Obviously, such free energy calculations also confirm the tendency of the Na^+ to accumulate within the PE layer in concentrations that is much more than that needed to screen the PE charges, which in turn leads to the occurrence of the overscreening effect.

In this context, we also study what happens for the system N3, where the cations are the Cs^+ ions. Cs^+ ions are found to neutralize only around 53% of the O of COO^- of the PE brush layer. Two factors are responsible for it with both being related to the size of the Cs^+ ions. Cs^+ ion is larger than Na^+ ion. As a result, much lesser amount of Cs^+ ions can enter the PE brush layer (being driven by the osmotic pressure in the bulk), as discussed above. Secondly, again due to the large size of the Cs^+ ions, the first peak of the O-Cs rdf (radial distribution function) is very far from the location of the peak of the O-Na rdf [see Fig. 6(E)]. More interesting is the fact that the first peak of the O-Cs rdf occurs at a distance (from O of the COO-) that is similar to the distance (from O of the COO-) where the second peak of the O-H_{water} rdf occurs [see Fig. 6(F)]. Therefore, if anything, Cs^+ ion will only be capable of replacing the H_{water} from the second solvation shell of O of COO^-. This implies that Cs^+ ions are unable to replace the neutralizing H_{water} of the *first* solvation shell of the O atoms of COO^-. The energy gain associated with replacing the neutralizing H_{water} from the second solvation shell by Cs^+ ions is significantly smaller than the energy gain associated with replacing the neutralizing H_{water} from the first solvation shell by the Na^+ ions, stemming from the fact that H_{water} in the first solvation is much more tightly bound to the O of COO^-. So the possible energy favorability associated with the Cs^+ ions remaining localized (*via* electrostatic attraction) within the PE brush layer is significantly smaller as compared to the Na^+ ions remaining localized (*via* electrostatic attraction) within the PE brush layer. Accordingly, a significantly more number of Na^+ ions can be present within the PE brush layer thereby leading to eventual overscreening, while the number of Cs^+ ions that can remain localized within the PE brush layer is much less and hence there is no overscreening for the case N3.

We want to conclude this section with a discussion on the effect of the degree of ionization of the PAA brushes on the possible overscreening effect. It is known that PAA is a weakly dissociating

polymer, although its degree of ionization depends on several parameters like the pH of the solvent, the concentration of the added salt, *etc*. For example, at a pH value that is above its pKa (~5), PAA is likely to be highly ionized,[54] which will be similar to what is considered in our study. On the other hand, in a prior all-atom MD simulation study,[55] we showed that the extent of Na^+ counterion condensation in the PE brush remained very high even for weakly ionized PAA brushes. For example, even with f=0.25 (where f is the ratio of the deprotonated functional groups to the total number of functional groups of the PAA chains; therefore f=0 implies a neutral PAA brush, while f=1 implies a fully ionized PAA brush), we found that more than 90% of the counterions were condensed on the PAA chains.[55] Such a large extent of counterion condensation will imply that even for weakly ionized PAA brushes, $–COO^-Na^+$ interactions (in presence of Na^+ screening counterions) will make a significant contribution to the overall free energy of the system. As discussed above, such a strong counterion-(PE-functional-group) interaction is a major driver of the overscreening effect. Therefore, we believe that even for the case of a nanochannel grafted with weakly ionized PAA brushes, the strong $–COO^-Na^+$ interactions will ensure that there will be overscreening effect within the PAA brush layer.

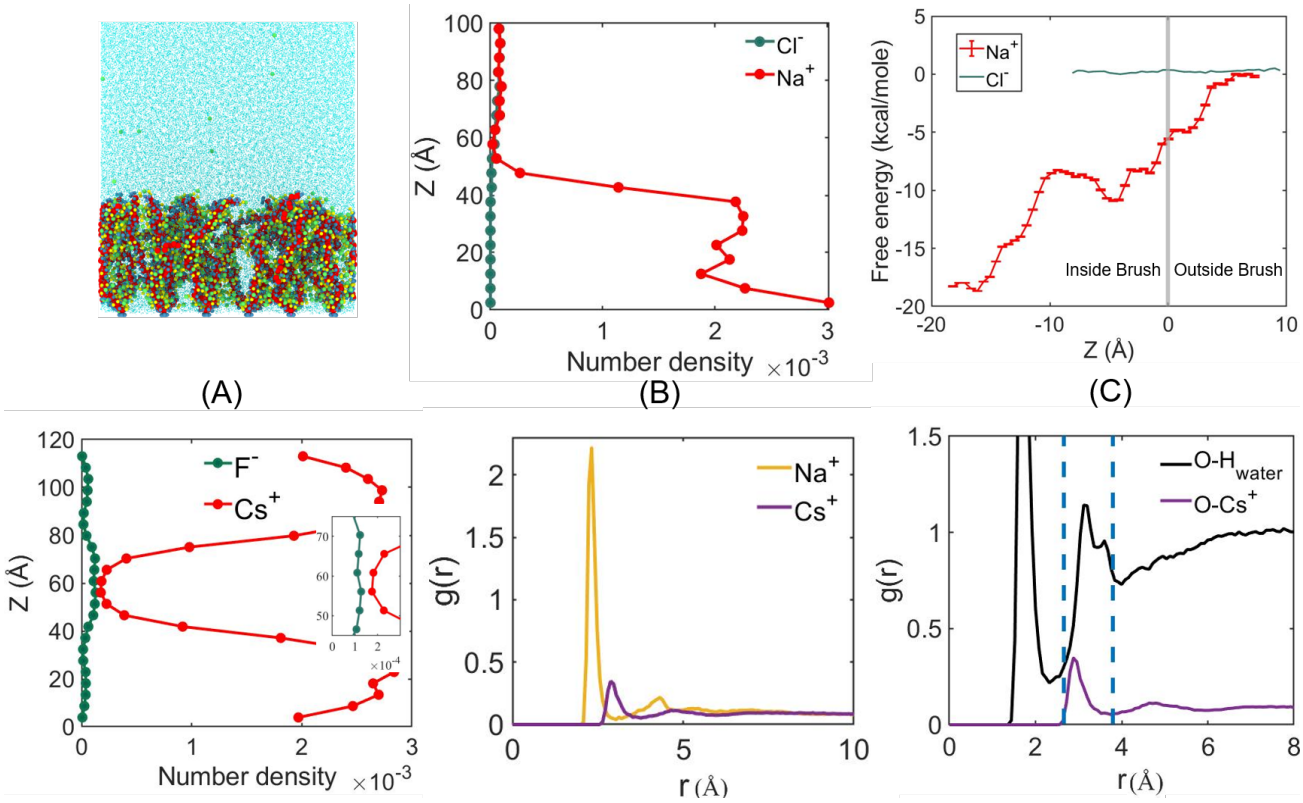

Figure 6: (A) Simulation snapshot of the simulation without any confinement where PE brushes are grafted to a single interface (system N2). (B) Ion distribution profile for the system without confinement (system N2) (Y axis is truncated after 100 Å). (C) Free energy curves of Na^+ and Cl^- ions with Z coordinates of the ion serving as the reaction coordinates. These free energies are obtained from the simulation with nanochannel and NaCl salt (system N1). Here, Z=0 roughly indicates the interface of brush layer and brush-free bulk. For the curve corresponding to the Cl^- ion, the size of the error bar is less than the line thickness. (D) Ion distribution profile for system N3 (nanochannel grafted with PAA brush layers with CsF as added salt). (E) RDF of Na^+ and Cs^+ with O^- of carboxylate group. (F) RDF of H and Cs^+ with O^- of carboxylate group. The location of the first peak of the O^-- Cs^+ RDF is indicated with dashed line [Y axis is truncated after g(r)=1.5].

Experimental relevance of the Present Study

Charge inversion or overscreening is observed in experiments involving silicone nanochannels[56,57] in presence of large concentrations of salts with multivalent ions. Overpopulation of multivalent counterions in the Stern layer adjacent to nanochannel wall causes the overscreening. On the other hand, in our study we have observed this overscreening with monovalent counterions, where the interplay of the presence of a strong nanoconfinement and the presence of the densely grafted charged PE brushes create an environment that force an accumulation of more than required counterions within the PE brush layer and triggers overscreening. Also, in these studies,[56,57] this overscreening scenario cannot be altered by the application of electric field, while in our study we can make the overscreening disappear at significantly larger electric field. A recent experiment, coupled with DFT calculations on protein−spherical nucleic acid conjugates, showed that above a certain salt concentration, a monovalent cation (Rb^+) can overcompensate the negative charges of the DNA molecules (densely grafted on gold nanoparticles), thereby causing an overscreening-like scenario.[58] This study, along with our all-atom MD simulation results demonstrating overscreening in presence of monovalent Na^+ screening counterions, suggest that explicit solvent all-atom MD simulations and quantum calculations can potentially play an important role in furthering our understanding of the overscreening of local charges of polyelectrolyte molecules even in presence of monovalent counterions.

It is well known that in a nanochannel due to the surface charge of the wall, there will be an electric double layer or an EDL and hence an imbalance in the number density of the positive and negative ions within the EDL: in presence of an applied electric field, the mobile ions are transported and this imbalance ensures that the water molecules are transported in the direction of

the migration of the ions that are larger in number within the EDL. For our case, at low electric field strengths, the presence of the overscreening effect within the PE brush layer implies that the coions are excess in number in the bulk and hence the EOS transport, in presence of the applied electric field, occurs in the direction of migration of the coions. Therefore, for this case, we indeed find that the EOS (electroosmotic) motion occurs due to the imbalance in the number of coions and counterions, albeit for the classical scenario the EOS transport primarily occurs due to the excess of counterions within the EDL. On the other hand, for larger electric field, the overscreening within the PE brush layer becomes negligible and there is equal number coions and counterions within the bulk: under such circumstances, the EOS transport occurs (in the direction of migration of the counterions) due to the larger residence time of water molecules within the counterions (Na^+ ions) than the coions (Cl^- ions). Therefore, the key mechanism of our reported EOS transport at large electric fields is different from that of the classical EOS transport. Despite that, the order of magnitude of our reported EOS transport at large electric fields is very similar to that reported in our previous experiments. For example, the EOS mobility, which is defined as EOS velocity per unit applied electric field has been reported to be in the order of $(1-10)\times 10^{-9}\ m^2/(Vs)$ for experiments,[40-41,59] while that computed for our simulations (for large electric field strength of 1 V/nm) is ~ $5.5\times 10^{-9}\ m^2/(Vs)$.

Also, in an experimental setup, there can be a reservoir of solution connected to a nanochannel and water and ions can move from the nanochannel to the reservoir and vice versa. To check the effect of reservoir in the overscreening scenario, we have performed one more simulation where the nanochannel is connected to two reservoirs at its two ends. We find that the density of coions are larger within the bulk, confirming the occurrence of overscreening within the

PE brush layer of the nanochannel even when the nanochannel is connected to two reservoirs on its two ends. Details of the simulation and results are given in the SI (figure S10 and section S6).

Conclusion:

In summary, our study shows (a) overscreening within the PE brush layer for zero or small electric field even in presence of monovalent counterions, (b) coion-dictated EOS velocity for smaller electric field, and (c) counterion-dictated EOS velocity field for larger electric field (which also indicates an electric field strength mediated switching of the direction of EOS transport) in nanochannels grafted with PE brushes. All these facets are dictated by an intricate interplay of the electric field driven (a) reduction in brush height caused by the electric field mediated preferential alignment of the brushes, (b) variation in velocities (mobilities) of coions (Cl^-) and counterions (Na^+), and (c) variation in residence times of the water molecules within the first solvation shells of the Cl^- and Na^+ ions. We anticipate that the findings of the paper will not only inspire future, well-resolved atomistic exploration of electrohydrodynamics of functionalized nanochannels unraveling physics at the interface of soft matter, chemistry, fluid mechanics, and nanoscience, but will also enable designing nanodevices with a better and easy control over the associated flows.

Methods

Molecular Dynamics Simulations:

Our main simulation contains [shown in Fig. 1(A)], fully ionized Polyacrylic acid (PAA) chains (H[-CH_2-$CH(COO^-)$-]nCH3) as the polyelectrolytes and SPC/E water[60] molecules. Sodium (Na^+) counterions screen the PE brush charges. In addition, we add 0.1 M NaCl salt. PE chains are grafted with a grafting density of $0.05/\sigma^2$ (σ=3.5 Å, is the LJ distance parameter of backbone carbon atoms). This grafting density of PAA chains is within the range of experimentally reported[55] grafting densities of 0.12-2.15 chain/nm^2 (in the chain/nm^2 unit, the grafting density considered for our case is 0.408 chain/nm^2). Each chain has 49 backbone carbon atoms. Purely repulsive walls are placed at the top and the bottom of the system to prevent the mobile ions and water molecules from escaping the system. 90 PE chains are grafted on each wall in a 15*6 (x*y) array. The particle trajectories are calculated using the Velocity-Verlet algorithm, with a time step of 2 fs. Non-bonded interactions are modelled as the sum of a shifted-truncated 12-6 Lennard Jones potential (U_{LJ}) with a cut-off of 13Å. Long range Columbic interaction is calculated using a PPPM (particle-particle particle-mesh) algorithm.[61] The bonds and angles of water molecules are conserved by using the SHAKE algorithm.[62] Our simulation system consists of a total of 277340 atoms. Dimensions in x, y, and z directions are 23.5 nm, 9.4 nm, and 12 nm respectively. Periodic boundary conditions are applied in x and y directions while the fixed boundary condition is incorporated in z direction. Simulations are performed in LAMMPS[63] and OVITO[64] is used to visualize the simulation system.

The system is first run in the NP_zT ensemble (the subscript z signifies that only the channel height is allowed to change) to obtain the correct simulation box height at 300 K and 1 atm, by applying the Nosé-Hoover thermostat and barostat.[65,66] Subsequently, the system is equilibrated in

the NVT ensemble for 16 ns to obtain the correct equilibrium configuration of the system by applying the Langevin thermostat.[67] After initial equilibration, we have applied the electric field under the NVT ensemble to remove the heat dissipated due to the flow. NVT is applied only in the direction perpendicular to the axial electric field and to avoid a flow profile bias, we have removed bias velocity with the help of a binning method employed in a direction perpendicular to the flow field. For more caution, only polymers are thermostatted in the entire system, this mimics the experimental scenario where temperature can be controlled form the outer surface. Only, the water molecules and mobile ions in the extreme left quarter of the simulation domain (in the x-direction) were thermostatted as depicted in figure S1(A). These simulations are performed for 8 ns to get steady-state velocity profile followed by a 12 ns production run.

We have used the OPLS-AA[68] force field to model the brush molecules and employed Joung *et al*.[69] for calculating the potentials for the mobile ions. These vastly used parameters for monovalent ions[69] were adjusted to the solvation free energy of ions in water and the lattice energy of ionic crystals. OPLS force field, which is used to model the PE brush molecule, has been used for modeling a variety of polymer systems such as hydrocarbons,[70] proteins,[71] rubbers,[72] *etc*. as the most accurate force field parameter. Geometric mixing rules are used for the LJ interactions between dissimilar atoms, except for the ion-ion and ion -water interactions. For these ion-ion and ion-water, we have used Lorentz-Berthelot mixing rules to be consistent with Joung *et al.*[69]

To calculate free energy calculations in our main simulation setup [results shown in Fig. 6(C)], a Na^+ ion and a Cl^- ion located inside the brush layer have been chosen. These two ions are pulled out from brush layer to the bulk by specifying the reaction coordinate in Z direction that varies by 1 Å in every successive reaction coordinate. For Na^+ and Cl^- ions, 26 and 18 reaction coordinates are considered, respectively. These ions were constrained to their windows by a

harmonic potential with spring constant of 5 kcal/mol.Å^2. All these simulations lasted for 2 ns and the data collected from the last 1.5 ns was used for analysis. The axial positions of the sample molecules were outputted every 20 fs and the weighted histogram analysis method (WHAM)[73,74] was used to analyze the data generated from umbrella sampling.

Acknowledgement: This work has been supported by the Department of Energy Office of Science grant DE-SC0017741. The authors also gratefully acknowledge the Deepthought2 High-Performance Computing cluster at the University of Maryland that was used to run the simulations.

Supporting Information: Force field parameters and other details for the MD simulations (section S1); brush properties (section S2); water distribution (section S3); ionic properties (section S4); details of the simulations concerning generality of the overscreening (section S5); simulations for the case where there is an attached reservoir to a nanochannel (section S6). Supporting information document is available free of charge at http://pubs.acs.org.

Author Contributions: S.D. conceived the problem. T.H.P. and H.S.S. ran the simulations. T.H.P., H.S.S., and P.R.D., analyzed the data. T.H.P. and S.D. wrote the paper. All authors commented on the paper.

Reference:

[1] Plümper, O.; Botan, A.; Los, C.; Liu, Y.; Malthe-SØrenssen, A.; Jamtveit, B. Fluid-Driven Metamorphism of The Continental Crust Governed by Nanoscale Fluid Flow. *Nat. Geosci.* **2017**, *10*, 685–690.

[2] Zhu, Y.; Zhan, K.; Zhu, X. Interface Design of Nanochannels for Energy Utilization. *ACS Nano* **2018**, *12*, 908–911.

[3] van der Heyden, F. H. J.; Bonthuis, D. J.; Stein, D.; Meyer, C.; Dekker, C. Electrokinetic Energy Conversion Efficiency in Nanofluidic Channels. *Nano Lett.* **2006**, *6*, 2232–2237.

[4] Venkatesan, B. M.; Bashir, R. Nanopore Sensors for Nucleic Acid Analysis. *Nat. Nanotechnol.* **2011**, *6*, 615–624.

[5] Miles, B. N.; Ivanov, A. P.; Wilson, K. A.; Dogan, F.; Japrung, D.; Edel, J. B. Single Molecule Sensing with Solid-State Nanopores: Novel Materials, Methods, and Applications. *Chem. Soc. Rev.* **2013**, *42*, 15–28.

[6] Fang, R.; Zhang, H.; Yang, L.; Wang, H.; Tian, Y.; Zhang, X.; Jiang, L. Supramolecular Self-Assembly Induced Adjustable Multiple Gating States of Nanofluidic Diodes. *J. Am. Chem. Soc.* **2016***, 138*, 16372–16379.

[7] Liu, M.; Zhang, H.; Li, K.; Heng, L.; Wang, S.; Tian, Y.; Jiang, L. A Bio-Inspired Potassium and pH Responsive Double-Gated Nanochannel. *Adv. Funct. Mater*. **2015**, *25*, 421–426.

[8] Huang, X.; Kong, X. Y.; Wen, L.; Jiang, L. Bioinspired Ionic Diodes: From Unipolar to Bipolar. *Adv. Funct. Mater.* **2018**, *28*, 1801079.

[9] Zhang, Z.; Wen, L. P.; Jiang, L. Bioinspired Smart Asymmetric Nanochannel Membranes. *Chem. Soc. Rev.* **2018**, *47*, 322–356.

[10] Chang C.-C.; Yang, R.-J. Electrokinetic Mixing in Microfluidic Systems. *Microfluid. Nanofluid*. **2007,** *3*, 501–525.

[11] Shestopalov, I.; Tice, J. D.; Ismagilov, R. F.; Multi-Step Synthesis of Nanoparticles Performed on Millisecond Time Scale in a Microfluidic Droplet-Based System. *Lab Chip* **2004**, *4*, 316–321.

[12] Pamme, N. Continuous Flow Separations in Microfluidic Devices. *Lab Chip* **2007**, *7*, 1644–1659.

[13] Weisgrab, G.; Ovsianikov, A.; Costa, P. F. Functional 3D Printing for Microfluidic Chips *Adv. Mater. Technol.* **2019**, *4*, 1900275.

[14] Esfandyarpour, R.; DiDonatoc, M. J.; Yangd, Y.; Durmus, N. G.; Harrisd, J. S.; Davis, R. W. Multifunctional, Inexpensive, and Reusable Nanoparticle-Printed Biochip for Cell Manipulation and Diagnosis. *Proc. Natl. Acad. Sci. USA* **2017**, *114*, E1306–E1315.

[15] Chen, L.-C.; Wu, C.-C.; Wu, R.-G.; Chang, H.-C. Electroosmotic Flow Control in Microfluidic Chips Using a Self-Assembled Monolayer as the Insulator of a Flow Field-Effect Transistor, *Langmuir* **2012**, *28*, 11281–11285.

[16] Oh, Y.-J.; Gamble, T. C.; Leonhardt, D.; Chung, C.-H.; Brueck, S. R. J.; Ivory, C. F.; Lopez, G. P.; Petseva, D. N.; Han, S. M. Monitoring FET Flow Control and Wall Adsorption of Charged

Fluorescent Dye Molecules in Nanochannels Integrated into a Multiple Internal Reflection Infrared Waveguide. *Lab Chip* **2008**, *8*, 251–258.

[17] Hayes, M. A.; Kheterpal, I.; Ewing, A. G. Effects of Buffer pH on Electroosmotic Flow Control by an Applied Radial Voltage for Capillary Zone Electrophoresis. *Anal. Chem.* **1993**, *65*, 27–31.

[18] Barker, S. L. R.; Ross, D.; Tarlov, M. J.; Gaitan, M.; Locascio, L. E. Control of Flow Direction in Microfluidic Devices with Polyelectrolyte Multilayers. *Anal. Chem.* **2000**, *72*, 5925–5929.

[19] Stroock, A. D.; Weck, M.; Chiu, D. T.; Huck, W. T. S.; Kenis, P. J. A.; Ismagilov, R. F.; Whitesides, G. M. Patterning Electro-Osmotic Flow with Patterned Surface Charge. *Phys. Rev. Lett.* **2000**, *84*, 3314–3317.

[20] Celebi, A. T.; Cetin, B.; Beskok, A. Molecular and Continuum Perspectives on Intermediate and Flow Reversal Regimes in Electroosmotic Transport. *J. Phys. Chem. C* **2019**, *123*, 14024–14035.

[21] Gao, X.; Zhao, T.; Li, T. Controlling Flow Direction in Nanochannels by Electric Field Strength. *Phys. Rev. E* **2015**, *92*, 023017.

[22] Das, S.; Banik, M.; Chen, G.; Sinha, S.; Mukherjee, R. Polyelectrolyte Brushes: Theory, Modelling, Synthesis and Applications. *Soft Matter* **2015**, *11*, 8550–8583.

[23] Ali, M.; Yameen, B.; Neumann, R.; Ensinger, W.; Knoll, W.; Azzaroni, O. Biosensing and Supramolecular Bioconjugation in Single Conical Polymer Nanochannels. Facile Incorporation of

Biorecognition Elements into Nanoconfined Geometries. *J. Am. Chem. Soc.* **2008**, *130*, 16351–16357.

[24] Umehara, S.; Karhanek, M.; Davis, R. W.; Pourmand, N. Label-Free Biosensing with Functionalized Nanopipette Probes. *Proc. Natl. Acad. Sci. USA* **2009**, *106*, 4611–4616.

[25] Ali, M.; Ramirez, P.; Mafe, S.; Neumann, R.; Ensinger, W. A pH-Tunable Nanofluidic Diode with a Broad Range of Rectifying Properties. *ACS Nano* **2009,** *3*, 603–608.

[26] Vilozny, B.; Wollenberg, A. L.; Actis, P.; Hwang, D.; Singaram, B.; Pourmand, N. Carbohydrate-Actuated Nanofluidic Diode: Switchable Current Rectification in a Nanopipette. *Nanoscale* **2013**, *5*, 9214–9221.

[27] Ali, M.; Yameen, B.; Cervera, J.; Ramirez, P.; Neumann, R.; Ensinger, W.; Knoll, W.; Azzaroni, O. Layer-by-Layer Assembly of Polyelectrolytes into Ionic Current Rectifying Solid-State Nanopores: Insights from Theory and Experiment. *J. Am. Chem. Soc.* **2010**, *132*, 8338–8348.

[28] Yameen, B.; Ali, M.; Neumann, R.; Ensinger, W.; Knoll, W.; Azzaroni, O. Single Conical Nanopores Displaying pH-Tunable Rectifying Characteristics. Manipulating Ionic Transport with Zwitterionic Polymer Brushes. *J. Am. Chem. Soc.* **2009**, *131*, 2070–2071.

[29] ShamsiJazeyi, H.; Miller, C. A.; Wong, M. S.; Tour, J. M.; Verduzco, R. Polymer-Coated Nanoparticles for Enhanced Oil Recovery. *J. Appl. Polym.* **2014**, *131*, 40576.

[30] Yang, Q.; Li, L.; Zhao, F.; Han, H.; Wang, W.; Tian, Y.; Wang, Y.; Ye, Z.; Guo, X. Hollow Silica–Polyelectrolyte Composite Nanoparticles for Controlled Drug Delivery. *J. Mater. Sci.* **2019**, *54*, 2552–2565.

[31] Saraswathy, M.; Gong, S. Recent Developments in the Co-Delivery of siRNA and Small Molecule Anticancer Drugs for Cancer Treatment. *Mater. Today* **2014**, *17*, 298–306.

[32] Chen, G.; Das, S. Scaling Laws and Ionic Current Inversion in Polyelectrolyte-Grafted Nanochannels. *J. Phys. Chem. B* **2015***, 119*, 12714–12726.

[33] Chen, G.; Das, S. Electroosmotic Transport in Polyelectrolyte-Grafted Nanochannels with pH-Dependent Charge Density. *J. Appl. Phys.* **2015,** *117*, 185304.

[34] Cao, Q.; You, H. Electroosmotic Flow in Mixed Polymer Brush-Grafted Nanochannels. *Polymers* **2016**, *8*, 438.

[35] Cao, Q.; Tian, X.; You, H. Electrohydrodynamics in Nanochannels Coated by Mixed Polymer Brushes: Effects of Electric Field Strength and Solvent Quality. *Model. Simul. Mater. Sci. Eng*. **2018**, *26*, 035003.

[36] Cao, Q. Anisotropic Electrokinetic Transport in Channels Modified with Patterned Polymer Brushes. *Soft Matter* **2019**, *15*, 4132–4145.

[37] Wu, P.; Sun, T.; Jiang, X.; Kondrat, S. Hydrodynamic Properties of Polymers Screening the Electrokinetic Flow: Insights from a Computational Study. *Polymers* **2019**, *11*, 1038.

[38] Sachar, H.S.; Pial, T.H.; Desai, P. R.; Etha, S. A.; Wang, Y.; Chung, P. W.; Das. S. Densely Grafted Polyelectrolyte Brushes Trigger “Water-in-Salt”-Like Scenarios and Ultraconfinement Effect. *Matter* **2020**, *2*, 1509–1521.

[39] Haywood, D. G.; Harms, Z. D.; Jacobson, Stephen C. Electroosmotic Flow in Nanofluidic Channels. *Anal. Chem.* **2014**, *86*, 11174−11180.

[40] Wu, D.; Qin, J.; Lin, B. Self-Assembled Epoxy-Modified Polymer Coating on a Poly(dimethylsiloxane) Microchip for EOF Inhibition and Biopolymers Separation. *Lab Chip* **2007**, *7*, 1490–1496.

[41] Paratore, F.; Boyko, E.; Kaigala, G.V.; Bercovici, M. Electroosmotic Flow Dipole: Experimental Observation and Flow Field Patterning. *Phys. Rev. Lett.* **2019**, *122*, 224502.

[42] English, N. J.; Waldron, C. J. Perspectives on External Electric Fields in Molecular Simulation: Progress, Prospects and Challenges. *Phys. Chem. Chem. Phys.* **2015**, *17*, 12407–12440.

[43] Ly, H. K.; Sezer, M.; Wisitruangsakul, N.; Feng, J. J.; Kranich, A.; Millo, D.; Weidinger, I. M.; Zebger, I.; Murgida, D. H.; Hildebrandt, P. Surface-Enhanced Vibrational Spectroscopy for Probing Transient Interactions of Proteins with Biomimetic Interfaces: Electric Field Effects on Structure, Dynamics and Function of Cytochrome c. *FEBS J.* **2011**, *278,* 1382–1390.

[44] Heng, J. B.; Aksimentiev, A.; Ho, C.; Marks, P.; Grinkova, Y. V.; Sligar, S.; Schulten, K.; Timp, G. The Electromechanics of DNA in a Synthetic Nanopore. *Biophys. J.* **2006**, *90*, 1098–1106.

[45] Saitta, A. M.; Saija, F.; Giaquinta, P. V. *Ab Initio* Molecular Dynamics Study of Dissociation of Water under an Electric Field. *Phys. Rev. Lett*. **2012**, *108*, 207801.

[46] Stuve, E. M. Ionization of Water in Interfacial Electric Fields: An Electrochemical View. *Chem. Phys. Lett.* **2012**, *519–520*, 1–17.

[47] Netz, R. R. Nonequilibrium Unfolding of Polyelectrolyte Condensates in Electric Fields. *Phys. Rev. Lett.* **2003**, *90*, 128104.

[48] Netz, R. R. Polyelectrolytes in Electric Fields. *J. Phys. Chem. B* **2003,** *107*, 8208–8217.

[49] Winkler, R. G.; Gold, M.; Reineker, P. Collapse of Polyelectrolyte Macromolecules by Counterion Condensation and Ion Pair Formation: A Molecular Dynamics Simulation Study. *Phys. Rev. Lett.* **1998,** *80*, 3731–3734.

[50] Cassone, G.; Creazzo, F.; Giaquinta, P.V.; Saija, F.; Saitta, A.M. *Ab Initio* Molecular Dynamics Study of an Aqueous NaCl Solution Under an Electric Field. *Phys. Chem. Chem. Phys.* **2016,** *18,* 23164–23164.

[51] Wright, M.R. *An Introduction to Aqueous Electrolyte Solutions*, Wiley, Chichester, United Kingdom, **2007**.

[52] Larentzos, J. P.; Criscenti, L. J. A Molecular Dynamics Study of Alkaline Earth Metal−Chloride Complexation in Aqueous Solution. *J. Phys. Chem. B* **2008**, *112,* 14243–14250.

[53] Li, H.; Erbas, A.; Zwanikken, J.; de la Cruz, M. Ionic Conductivity in Polyelectrolyte Hydrogels. *Macromolecules* **2016**, *49*, 9239−9246.

[54] Hollingsworth, N. R.; Wilkanowiczbc, S. I.; Larson, R. G. Salt- and pH-Induced Swelling of a Poly (acrylic Acid) Brush *via* Quartz Crystal Microbalance w/Dissipation (QCM-D). *Soft Matter* **2019**, *15*, 7838–7851.

[55] Sachar, H. S.; Pial, T. H.; Desai, P. R.; Das. S. All-Atom Molecular Dynamics Simulations of Weak Polyionic Brushes: Influence of Charge Density on the Properties of Polyelectrolyte Chains, Brush Supported Counterions, and Water Molecules. *Soft Matter* **2020**, *16,* 7808–7822.

[56] Heyden, F. H. J. v. d.; Stein, D.; Besteman, K.; Lemay, S. G.; Dekker, C. Charge Inversion at High Ionic Strength Studied by Streaming Currents. *Phys. Rev. Lett.* **2006**, *96,* 224502.

[57] Besteman, K.; Zevenbergen, M. A. G.; Lemay, S. G. Charge Inversion by Multivalent Ions: Dependence on Dielectric Constant and Surface-charge Density. *Phys. Rev. E* **2005**, *72,* 061501.

[58] Krishnamoorthy, K.; Hoffmann, K.; Kewalramani, S.; Brodin, J. D.; Moreau, L. M.; Mirkin, C. A.; de la Cruz, M.; Bedzyk, M. J. Defining the Structure of a Protein−Spherical Nucleic Acid Conjugate and Its Counterionic Cloud. *ACS Cent. Sci.* **2018**, *4,* 378−386.

[59] Peng R.; Li, D. Electroosmotic Flow in Single PDMS Nanochannels. *Nanoscale* **2016**, *8*, 12237–12246.

[60] Berendsen, H. J. C.; Grigera J. R.; Straatsma T. P. The Missing Term in Effective Pair Potentials. *J. Phys. Chem.* **1987**, *91*, 6269–6271.

[61] Hockney, R. W.; Eastwood, J. W. *Computer Simulations Using Particles*. 1st Edition, Taylor and Francis, New York, **1988**.

[62] Ryckaert, J.-P.; Ciccotti, G.; Berendsen, H. J. Numerical Integration of the Cartesian Equation of Motion of a System with Constraints: Molecular Dynamics of n-Alkanes. *J. Comput. Phys.* **1977**, *23,* 327–341.

[63] Plimpton, S. Fast Parallel Algorithms for Short-Range Molecular Dynamics. *J. Comput. Phys.* **1995**, *117*, 1–19.

[64] Stukowski, A. Visualization and Analysis of Atomistic Simulation Data with OVITO—The Open Visualization Tool. *Model. Simul. Mater. Sci. Eng*. **2010**, *18*, 015012.

[65] Hoover, W.G. Canonical Dynamics: Equilibrium Phase-Space Distributions. *Phys. Rev. A* **1985**, *31*, 1695–1697.

[66] Nosé, S. A Unified Formulation of the Constant Temperature Molecular Dynamics Methods. *J. Chem. Phys.* **1984**, *81*, 511–519.

[67] Schneider, T.; Stoll, E. Molecular-Dynamics Study of a Three-Dimensional One-Component Model for Distortive Phase Transitions. *Phys. Rev. B* **1987**, *17*, 1302–1322.

[68] Jorgensen, W. L.; Maxwell, D. S.; Tirado-Rives, J. Development and Testing of the OPLS All-Atom Force Field on Conformational Energetics and Properties of Organic Liquids. *J. Am. Chem. Soc.* **1996**, *118*, 11225–11236.

[69] Joung, I. S.; Cheatham III, T. E. Determination of Alkali and Halide Monovalent Ion Parameters for use in Explicitly Solvated Biomolecular Simulations. *J. Phys. Chem. B.* **2008**, *112*, 9020–9041.

[70] Odegard, G. M.; Clancy, T. C.; Gates, T. S. Prediction of Mechanical Properties of Polymers with Various Force Fields. In *46th AIAA/ASME/ASCE/AHS/ASC Structures, Structural Dynamics and Materials Conference*, Austin, Texas, **2005**. doi.org/10.2514/6.2005-1850.

[71] Smith, M. D.; Rao, J. S.; Segelken, E.; Cruz, L. Force-Field Induced Bias in the Structure of Aβ21–30: A Comparison of OPLS, AMBER, CHARMM, and GROMOS Force Fields. *J. Chem. Inf. Model* **2015**, *55*, 2587–2595.

[72] Sharma, P.; Roy, S.; Karimi-Varzaneh, H. A. Validation of Force Fields of Rubber Through Glass-Transition Temperature Calculation by Microsecond Atomic-Scale Molecular Dynamics Simulation. *J. Phys. Chem. B* **2016**, *120*, 1367–1379.

[73] A. Grossfield, *WHAM: The Weighted Histogram Analysis Method*, version 2.0.9, Grossfield lab website, University of Rochester (http://membrane.urmc.rochester.edu/content/wham).

[74] Kumar, S.; Bouzida, D.; Swendsen, R. H.; Kollman, P. A.; Rosenberg, J. M. The Weighted Histogram Analysis Method for Free-Energy Calculations on Biomolecules. I. The Method. *J. Comput. Chem.* **1992**, *13*, 1011–1021.

Table of Content: